A Fast Wavelet Collocation Method for High-Speed Circuit Simulation

Dian Zhou and Wei Cai

***Abstract*—The advance of very large scale integration (VLSI) systems has been continuously challenging today's circuit simulators in both computational speed and stability. This paper presents a novel approach, the fast wavelet collocation method (FWCM), for high-speed circuit simulation. FWCM has the following properties: 1) it works in the time domain, so that circuit nonlinearity can be handled and numerical accuracy can be well controlled, unlike the method of working in the frequency domain where numerical error may become uncontrolled during the inverse *Laplace* transform; 2) the wavelet property of localization in both the time and frequency domains makes a uniform approximation possible, which is generally not found in time-marching methods; (3) it is very effective in treating singularities which often develop in high-speed ICs; (4) an adaptive scheme exists; and (5) it has an $O(h^4)$ convergence rate, where h is the step length. Numerical experiments further demonstrated the promising features of FWCM in high-speed IC simulation.**

***Index Terms*—Circuit simulation, VLSI, wavelet method.**

I. Introduction

THE existing numerical methods for the circuit simulation can be classified into two classes: time-marching and frequency-domain methods. The time-marching method is the most popular one because in the time domain circuit nonlinearity can be easily handled and design engineers often need to see the signal waveform directly [3]. However, the method suffers from the difficulty in effectively handling the singularity which often develops in high-speed circuits and the problem of nonuniform error distribution.

The challenge to the time-marching method in effectively handling system singularities has been well understood. From a numerical computation viewpoint, the rapid changing of signals in high-speed circuits implies severe singularity. To catch such fast-changing waveforms, the time-marching step length needs to be sufficiently reduced to maintain the stability and accuracy of the marching scheme, thus slowing down the computation [4].

The importance of the uniform approximation has not been thoroughly explored in the published literature. Let us illustrate this point by examining a real IC design and fabrication process. It is not unusual that a circuit parameter has a 10 to 50% deviation from its standard value, due to the uncontrollable factors in the chip fabrication process. A wire of 0.5 μm standard width can easily be fabricated 10% wider or narrower and so can its capacitance and resistance. Therefore, it is not necessary to compute the signal variables with a great deal of accuracy. What is really needed is to compute them with the same or slightly higher accuracy, achievable by the fabrication. However, most time-marching methods used in today's circuit simulators usually must set a very small error tolerance at early time steps (local truncation error control in SPICE simulation) to avoid a solution from diverging later. Otherwise, the error may accumulate during time marching and, consequently, cause the nonuniform error distribution over the entire time interval. For example, suppose that a 1% error margin is allowed at any time point for a circuit simulation. The time-marching method needs to keep a much smaller local truncation error in most time steps in order to achieve the given global error tolerance. This is true even for many implicit time-marching schemes which are stable for any step length. A severe phase shifting will occur if the solution accuracy is not adequate at early time steps [3], [4]. Fig. 1 demonstrates such an instance where the Euler forward method does not converge and the Runge–Kutta method introduces a noticeable phase shifting because of the large time steps (related to the accuracy).

As is seen, to avoid the diverging and phase shifting caused by nonuniform error distribution, time-marching methods need to compute with an unnecessarily high accuracy in the early time steps. It, in turn, wastes much computation time. Such an effort is not required by the original circuit simulation problem, but is made for the sake of the chosen numerical techniques. Significant computation time can be saved if a numerical method has the property of producing a solution with a uniform error distribution.

As far as the frequency-domain method is concerned, the uniform error distribution can be achieved because, unlike the physical quantity time, frequency does not have a particular direction. The well-known asymptotic waveform evaluation (AWE) method is a good example of this type of method [8]. Unfortunately, the error in the frequency domain may become amplified during the inverse transform from the frequency domain back to the time domain. This has been a key drawback for the frequency-domain methods [9], [10]. Fig. 2 pictorially illustrates the undesired error amplification introduced by the domain transform.

The motivation for using wavelets for the simulation of high-speed VLSI circuits relies on the following observation.

Manuscript received May 15, 1996; revised August 9, 1998. The work of D. Zhou was supported in part by the NSF NYI under Grant MIP-9457402. The work of W. Cai was supported in part by ARPA under Grant F49620-96-1-0341 and in part by AFOSR under Grant F49620-96-1-0412. This paper was recommended by Associate Editor U. Feldmann.

D. Zhou is with The Department of Electrical Engineering, The University of North Carolina at Charlotte, Charlotte, NC 28269 USA (e-mail: zhou@uncc.edu).

W. Cai is with The Department of Mathematics, The University of North Carolina at Charlotte, Charlotte, NC 28269 USA (e-mail: wcai@uncc.edu).

Publisher Item Identifier S 1057-7122(99)06363-1.

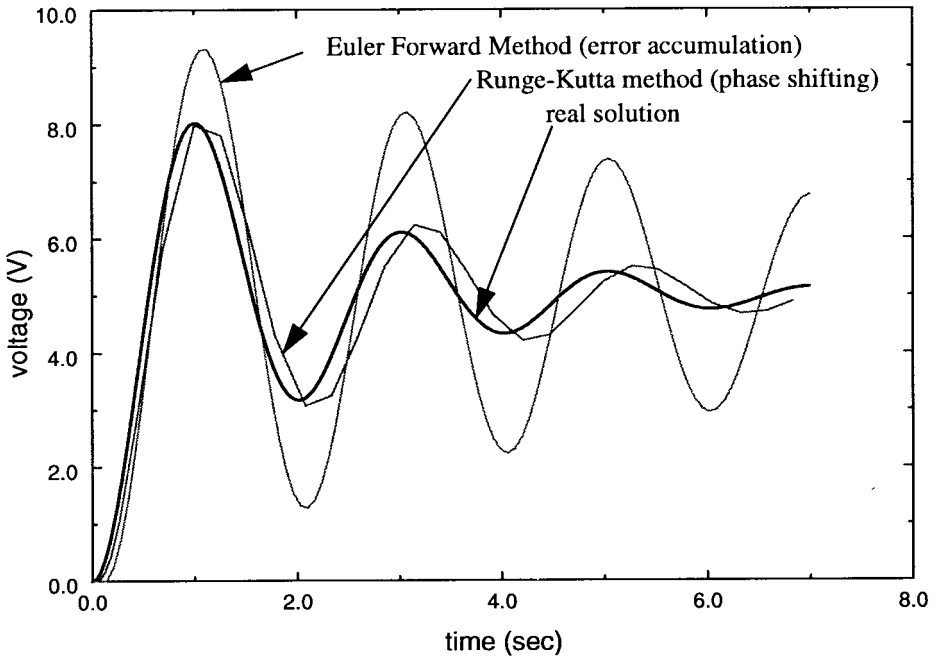

Fig. 1. Nonuniform error distribution and phase shifting of the time-marching methods.

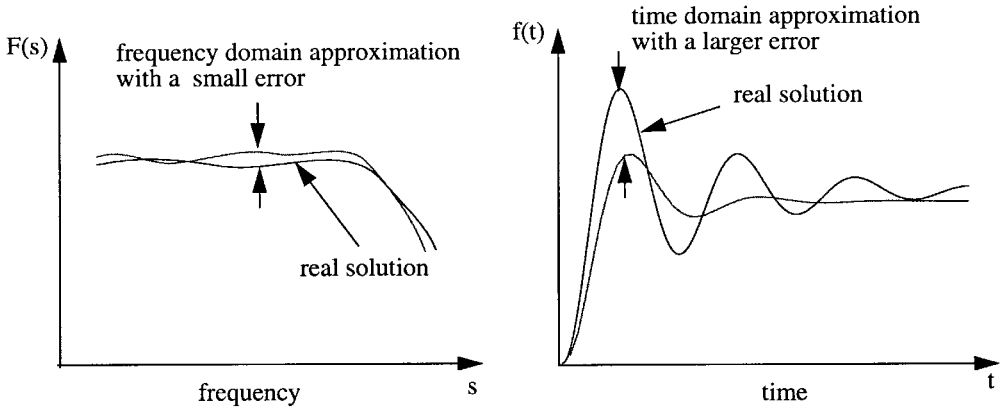

Fig. 2. Uncontrollable amplification of error during the domain transform.

As we know, wavelets have been widely used for image compression where sharp image edges must be represented efficiently. Notice that those sharp edges correspond to fast-changing signals. We can actually use wavelets to decompose solutions of ordinary differential equations (ODE's) which describe VLSI systems. Wavelet basis functions will provide a nice adaptive approach, which maintains a uniform approximation to resolve the singularities of a function [2], [12], [13]. Such a uniform approximation is made possible by the multiresolution properties of wavelet expansions of functions and the local compactness of wavelet basis functions. The key feature in the wavelet approximation is the fact that wavelet basis functions with compact support and higher frequency components are only used near the singularities, thus providing a uniform error distribution for the wavelet approximations.

We shall develop a fast wavelet collocation method which works in the time domain and provides a uniform error distribution [2]. The method is extremely powerful in treating singularity because of the wavelet property, localization, in both frequency and time domains and has a fourth-order convergence rate [2]. Although the complete mathematical discussion of the wavelet collocation method for partial differential equations (PDE's) was given in [2] and the method's general properties for ODE's were presented in [1], many researchers still found it difficult to apply such an approach to their applications since it is sheerly new to electrical engineering circles and nonmathematical literature on the subject seldom exists. To address this situation, we shall present a relatively detailed construction of FWCM, the treatment of initial conditions of ODE's, and the implementation necessary to make the paper self contained. All mathematical proofs of the FWCM are left to [1] and [2], for they are not the objective of this paper.

This paper will focus on the FWCM for linear ODE's. The extension of the FWCM to nonlinear systems is discussed in a sequel paper [7], [11], due to limitations in space here. Therefore, we shall emphasize the method's theoretical framework rather than the detailed numerical treatments. In

Section II we first introduce the basic concept of wavelets and the function expansion by using wavelets. We then develop an interpolation scheme for solving ordinary differential equations. In Section III we compare the FWCM with the other circuit simulation methods, based on both theoretic analysis and numerical experiments. In Section IV we comment on the future research. Finally, in the Appendix, we briefly show the properties of Sobolev space used in this paper.

II. The FWCM for ODEs

Without loss of generality, we assume that a circuit is described by an ordinary differential equation of the type

$$\frac{dx}{dt} = f(t,x), \tag{2.0a}$$

$$x(0) = x_0 \tag{2.0b}$$

where $x(t) = (x_1(t), x_2(t), \ldots, x_n(t))$ is an unknown vector function, $f(t,x)$ is a given nonlinear vector function, and $x(0)$ specifies the initial condition. We are interested in the solution of x in a finite interval $I = [0, L]$. For simplicity, we assume that $L > 4$. (A scaling operation can be applied to the interval I to cover any intervals required.)

The idea behind the wavelet collocation method is quite simple. We expand the unknown function x by a wavelet series and let the expansion satisfy the original ODE at the chosen collocation points, to determine the expansion coefficients. Unlike the wavelets used in the image processing, we need to construct the wavelets which are not only able to represent a signal in the interior of an interval, but also the arbitrary boundary conditions (including the signal's derivative). Before applying FWCM to any practical problem, the following basic problems need to be addressed; the introduction of approximation subspaces, the construction of the basis functions, the treatment of initial conditions, the expansion of the known functions, and the transform between the expansion coefficients and functions at the collocation points. In the following, we first present the theory of using wavelets to expand an arbitrary function and then show how to use this expansion to construct the solution of an ODE.

A. Function Expansion

Let $H^2(I)$ be the Sobolev space which basically contains functions with square integrable second derivatives [5]. We first introduce approximation subspace $V_{bJ} \subset H^2(I)$ for a given integer $J \geq 0$ and a fixed interval $I = [0, L]$, consisting of scaling functions and wavelet functions

$$\begin{aligned} V_{bJ} = \{&\eta_1(t), \eta_2(t), \eta_2(L-t), \eta_1(L-t) \\ &\varphi_{0,-1}(t), \varphi_{0,0}(t), \ldots, \varphi_{0,L-4}(t), \varphi_{0,L-3}(L-t) \\ &\psi_{0,-1}(t), \psi_{0,0}(t), \psi_{0,1}(t), \ldots, \psi_{0,n_0-3}(t), \psi_{0,n_0-2}(t) \\ &\cdots\cdots\cdots\cdots \\ &\psi_{j,-1}(t), \psi_{j,0}(t), \psi_{j,1}(t), \ldots, \psi_{j,n_j-3}(t), \psi_{j,n_j-2}(t) \\ &\cdots\cdots\cdots\cdots \\ &\psi_{J-1,-1}(t), \psi_{J-1,0}(t), \psi_{J-1,1}(t), \ldots, \psi_{J-1,n_{J-1}-3}(t) \\ &\psi_{J-1,n_{J-1}-2}(t)\}. \end{aligned} \tag{2.1}$$

The scaling functions in (2.1) are boundary scaling functions

$$\begin{aligned} \varphi_{0,-1}(t) &= \varphi_b(t) \\ &= \frac{3}{2}t_+^2 - \frac{11}{12}t_+^3 + \frac{3}{2}(t-1)_+^3 \\ &\quad - \frac{3}{4}(t-2)_+^3 + \frac{1}{6}(x-3)_+^3 \end{aligned} \tag{2.2a}$$

$$\varphi_{0,L-3}(L-t) = \varphi_b(L-t) \tag{2.2b}$$

and the interior scaling functions

$$\varphi_{0,k}(t) = \varphi(t-k), \quad 0 \leq k \leq L-4 \tag{2.2c}$$

where

$$\varphi(t) = N_4(t) = \frac{1}{6}\sum_{l=0}^{4}\binom{4}{l}(-1)^l(t-l)_+^3 \tag{2.2d}$$

$$t_+^n = \begin{cases} t^n, & \text{if } t \geq 0 \\ 0, & \text{otherwise} \end{cases}$$

and $N_4(t)$ is the fourth-order B-spline [6].

The functions $\eta_1(t)$, $\eta_2(t)$ are used to handle nonhomogeneity of the boundary data

$$\eta_1(t) = (1-t)_+^3 \tag{2.3a}$$

$$\eta_2(t) = 2t_+ - 3t_+^2 + \frac{7}{6}t_+^3 - \frac{4}{3}(t-1)_+^3 + \frac{1}{6}(t-2)_+^3. \tag{2.3b}$$

The boundary wavelet functions are

$$\psi_{j,-1}(t) = \psi_{b0}(2^j t), \qquad \psi_{j,0}(t) = \psi_{b1}(2^j t) \tag{2.4a}$$

$$\psi_{j,n_j-3}(t) = \psi_{b1}(2^j(L-t)), \qquad \psi_{j,n_j-2}(t) = \psi_{b0}(2^j(L-t)) \tag{2.4b}$$

where

$$\psi_{b0}(t) = -\frac{56}{99}(14\psi_{0,-2}(t) + \psi_{0,-1}(t)) \tag{2.4c}$$

$$\psi_{b1}(t) = \frac{182}{181}\left(\psi(t) + \frac{1}{13}(\psi_{0,-1}(t) + \psi_{0,-2}(t))\right) \tag{2.4d}$$

$$\psi_{0,-1}(t) = \psi(t+1), \quad \psi_{0,-2}(t) = \psi(t+2) \tag{2.4e}$$

and the interior wavelet functions are

$$\psi_{j,k}(t) = \psi(2^j t - k), \qquad k = 1, \ldots, n_j - 4 \tag{2.4f}$$

where $n_j = 2^j L$ and

$$\psi(t) = -\frac{3}{7}\varphi(2t) + \frac{12}{7}\varphi(2t-1) - \frac{3}{7}\varphi(2t-2). \tag{2.4g}$$

The total number of basis functions in (2.1) is $N = L+3+\sum_{j=0}^{J-1} 2^J L = 2^J L + 3$. Fig. 3 plots all those functions. Please note that all of them have nonzero values only in a small time interval. This property is referred to as the localization in time domain or local support.[1]

[1] Fourier basis e^{ikt} is not localized in the time domain and has a global support.

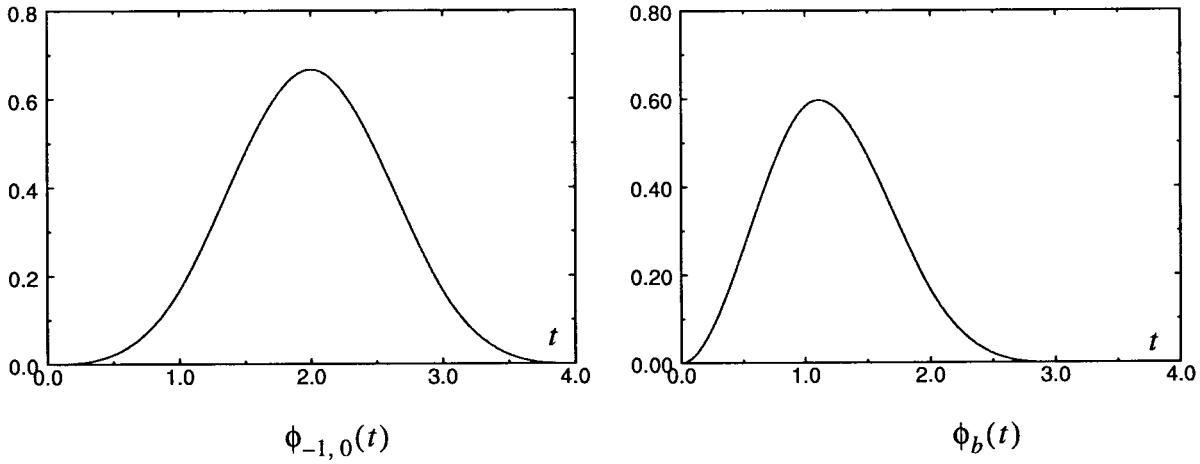

(a)

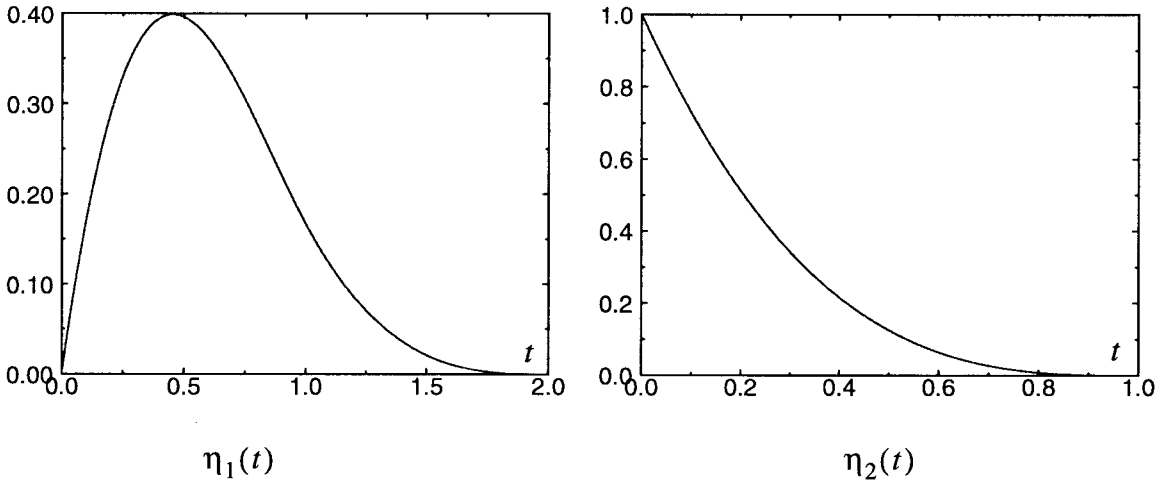

(b)

Fig. 3. (a) Two scaling functions. (b) Base wavelets.

We further define a set of subspaces

$$V_b = \{\eta_1(t),\ \eta_2(t),\ \eta_2(L-t)\ \eta_1(L-t)\}, \tag{2.5a}$$

$$V_0 = \text{span}\{\varphi_{0,-1}(t),\ \varphi_{0,k}(t),\ 0 \le k \le L-4\ \varphi_{0,L-3}(L-t)\} \tag{2.5b}$$

$$W_j = \text{span}\{\psi_{j,k}(t),\ -1 \le k \le n_j - 2\}, \qquad 0 \le j \le J-1 \tag{2.5c}$$

$$V_j = V_0 \oplus W_0 \oplus W_1 \oplus \cdots \oplus W_{j-1}, \qquad 0 \le j \le J-1 \tag{2.6}$$

$$V_{bj} = V_b + V_j \tag{2.7}$$

where the notation $V \oplus W$ stands for the direct sum $\text{span}\{f_1, f_2, \ldots, f_n\}$ representing a function set formed by all linear combinations of the functions of $f_1, f_2, \ldots, f_n$.

Among the functions defined above, $\varphi_{0,-1}(t)$ and $\varphi_{0,L-3}(L-t)$ are called boundary scaling functions, $\varphi_{0,k}(t)$ is called an interior scaling function and, together, they form a base interpolation space V_o. Functions $\psi_{j,k}(t)$ are wavelets where indexes j and k, respectively, represent the operations of dilation and translation. The dilation generates high-frequency wavelets and the translation moves wavelets to cover the whole physical time space, as illustrated in Fig. 4. Wavelets with the same dilation index j form a wavelet subspace level W_j. The Sobolev space is then decomposed into levels, with the jth level represented by the wavelets in W_j. This is similar to the situation in the Fourier series representation, where the space is decomposed into frequency subspaces. When using wavelets as the basis functions to approximate an arbitrary function, we can insert the wavelets at the needed physical time location by the translation operation and go to any high resolution (frequency) by the dilation. As a result, we can achieve any high resolution at any physical location as we wish. This is the key factor in achieving the uniform approximation computation since we can always insert high-frequency wavelets to the place (time points) where the prescribed accuracy has not been achieved. In contrast, such a nice property is not shared by the Fourier series, where basis functions are not localized in time. The insertion of one base Fourier function will affect the approximation over the entire time interval.

For the wavelet set introduced, we can prove the following properties [2]:

$$V_0 \subset V_1 \subset V_2 \subset \ldots$$

where $V_j = V_{j-1} + W_{j-1}$, $j \ge 1$.

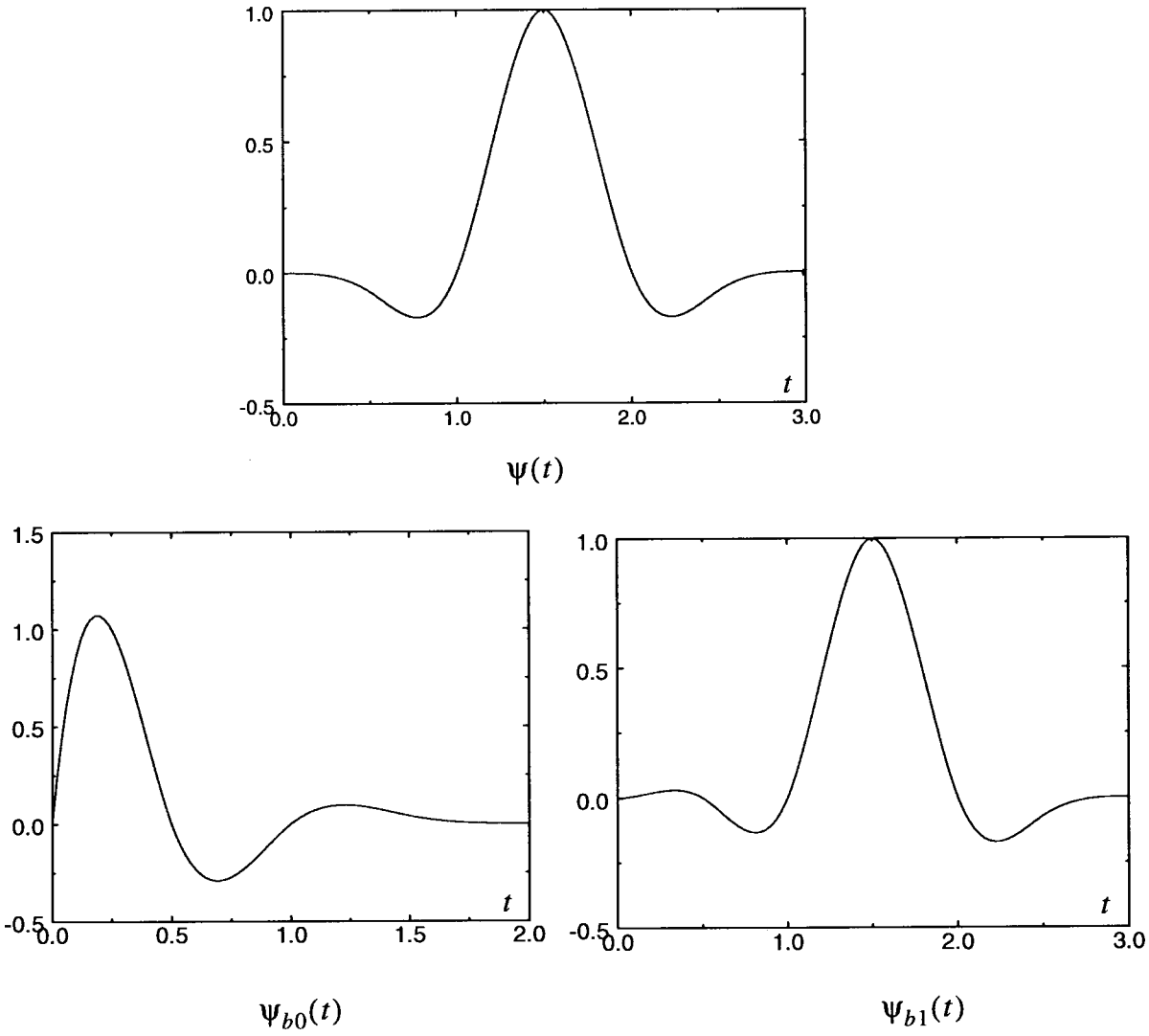

(c)

Fig. 3. *(Continued.)* (c) Base wavelets.

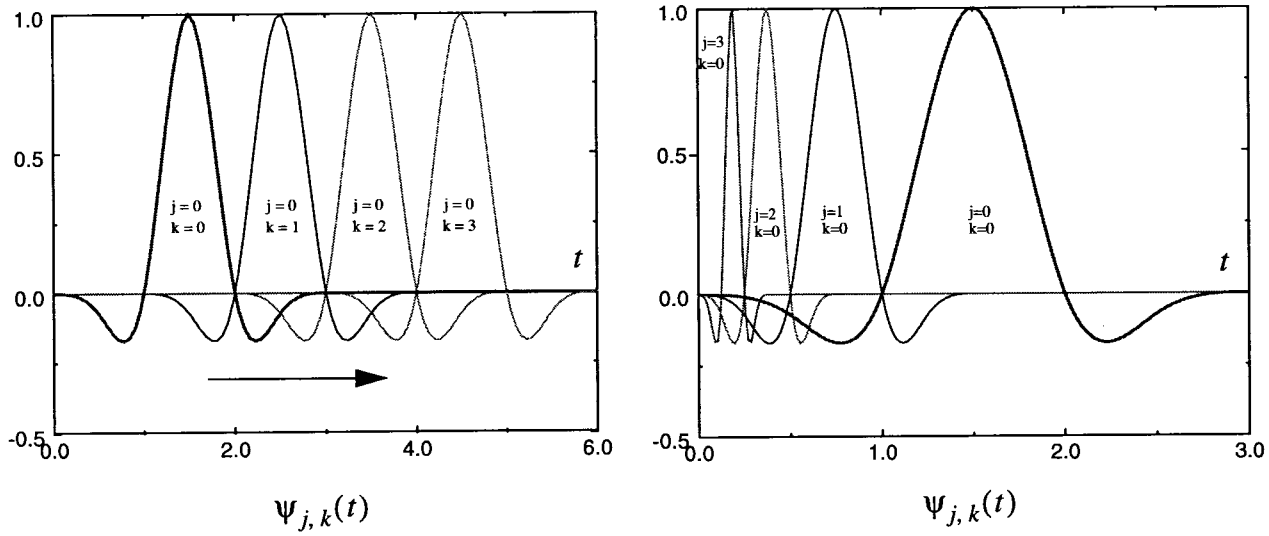

Fig. 4. The operations of dilation and translation on the base wavelets.

Also

(i)

$$V_{j+1} = V_j \oplus W_j, \qquad \text{for } j \in Z^+$$

(ii)

$$W_j \perp W_{j+1}, \quad j \in Z^+, \qquad \text{and}$$

$$H_0^2(I) = V_0 \oplus_{j \in Z^+} W_j$$

where Z^+ is the positive integer set. $H_0^2(I)$ is the subspace of $H^2(I)$ with homogeneous (zero) boundary data on interval I.

With the above properties, any function $x(t) \in H_0^2(I)$ can be approximated as closely as needed by a function $x_j(t) \in V_j = V_0 \oplus W_0 \oplus W_1 \oplus \cdots \oplus W_{j-1}$ for a sufficiently large j. In this case, the approximation relates to a homogeneous problem, i.e., $x(0) = x(L) = 0$. For any function $x(t) \in H^2(I)$, $x(0) \neq 0$, $x(L) \neq 0$ we have introduced a set of boundary functions $V_b = \{\eta_1(t), \eta_2(t), \eta_2(L-t), \eta_1(L-t)\}$, as defined in (2.5a) and (2.5b). If we use V_b to approximate boundary values of $x(t) \in H^2(I)$, then $x_j(t) \in V_b \cup V_j$ will still have an approximation to $x(t)$ of order $O(2^{-4j})$ for a given $j \geq 0$ [2]. The present approximation will be used to treat the nonhomogeneous problem. For simplicity, we denote $V_{bj} = V_b \cup V_j$, $j \geq 0$.

It must be pointed out that the boundary functions[2] $\eta_1(t)$, $\eta_2(t)$ and $\eta_2(L-t)$, $\eta_1(L-t)$ are essential in treating the boundary conditions. We use $\eta_1(t)$ to deal with the values of unknown functions at boundary points and $\eta_2(t)$ to the values of derivative functions. For either homogeneous or nonhomogeneous problem, functions $\eta_1(t)$, $\eta_2(t)$ and $\eta_2(L-t)$, $\eta_1(L-t)$ are always needed, since all other basis functions and their derivatives vanish at the boundary points of the interval I (see Fig. 3). This explains why we use the basis functions (2.1) in the subspace $V_{bj} \subset H^2(I)$, instead of $V_j \subset H_0^2(I)$ defined by $H_0^2(I) = \{x \in H^2(I) \mid (x(0) = x(L) = x'(0) = x'(L) = 0)\}$ [5]. Hereafter, we will consider the homogeneous or nonhomogeneous problem with a universal framework.

B. System Discretization

For any function $x(t) \in H^2(I)$, we expand it by means of the basis function system defined by (2.1) and consider its interpolation at some interior knots, called collocation points, defined below. We write the expansion of the function $x(t)$ as

$$x_J(t) = I_{V_{b0}} x(t) + \sum_{j=0}^{J-1} I_{W_j} x(t) \tag{2.8}$$

where

$$\begin{aligned} I_{V_{b0}} x(t) &= \hat{x}_{-1,-3}\eta_1(t) + \hat{x}_{-1,-2}\eta_2(t) \\ &\quad + \hat{x}_{-1,-1}\varphi_b(t) + \sum_{k=0}^{L-4} \hat{x}_{-1,k}\varphi_k(t) \\ &\quad + \hat{x}_{-1,L-3}\varphi_b(L-t) \\ &\quad + \hat{x}_{-1,L-2}\eta_2(L-t) + \hat{x}_{-1,L-1}\eta_1(L-t) \\ &= x_{-1}(t) \in V_{b0} \end{aligned} \tag{2.9}$$

[2]The left boundary of a time interval is the initial time point of the ODE's.

and

$$I_{W_j} x(t) = \sum_{k=-1}^{n_j-2} \hat{x}_{j,k}\psi_{j,k}(t) = x_j(t) \in W_j, \quad 0 \leq j \leq J-1. \tag{2.10}$$

Denote expansion coefficients by a vector

$$\begin{aligned} \hat{x}_J = \big(&\hat{x}_{-1,-3}, \hat{x}_{-1,-2}, \ldots, \hat{x}_{-1,k}, \ldots, \hat{x}_{-1,L-2}, \hat{x}_{-1,L-1} \\ &\hat{x}_{0,-1}, \hat{x}_{0,0}, \ldots, \hat{x}_{0,k}, \ldots, \hat{x}_{0,n_o-3}, \hat{x}_{0,n_o-2}; \cdots\cdots\cdots \\ &\hat{x}_{J-1,-1}, \hat{x}_{J-1,0}, \ldots, \hat{x}_{J-1,k}, \ldots, \hat{x}_{J-1,n_{J-1}-3}, \\ &\hat{x}_{J-1,n_{J-1}-2}\big) \end{aligned} \tag{2.11}$$

which will be determined by satisfying interpolating conditions at collocation points $t_k^{(-1)}$, $1 \leq k \leq L+3$ and $t_k^{(j)}$, $-1 \leq k \leq n_j - 2$, $j \geq 0$, i.e.,

$$\begin{cases} I_J x\big(t_k^{(-1)}\big) = x\big(t_k^{(-1)}\big), & 1 \leq k \leq L+3 \\ I_J x\big(t_k^{(j)}\big) = x\big(t_k^{(j)}\big), & \\ \qquad\qquad j \geq 0, \quad -1 \leq k \leq n_j - 2, & 0 \leq j \leq J-1 \end{cases} \tag{2.12}$$

The following collocation points are chosen for V_{b0} and W_j, $j \geq 0$, respectively.

$$t_1^{(-1)} = 0, \quad t_2^{(-1)} = \frac{1}{2}, \quad t_k^{(-1)} = k-2, \quad 3 \leq k \leq L+1$$

$$t_{L+2}^{(-1)} = L - \frac{1}{2}, \qquad t_{L+3}^{(-1)} = L \tag{2.13a}$$

$$t_{-1}^{(j)} = \frac{1}{2^{j+2}}, \quad t_k^{(j)} = \frac{k+1.5}{2^j}, \qquad 0 \leq k \leq n_j - 3$$

$$t_{n_j-2}^{(j)} = L - \frac{1}{2^{j+2}}. \tag{2.13b}$$

Again, the total number of collocation points is $N = 2^J L + 3$, which equals exactly the number of the basis functions defined in (2.1) and the number of the expansion coefficients in (2.11). Therefore, the derivative values of $x_J(t)$ in (2.8) at collocation point $\{t_k^{(j)}\}$ are denoted by $\dot{x}_J$ and related to the expansion coefficient $\hat{x}_J$ by a so-called derivative matrix $A = (a_{ij})$, i.e.,

$$\dot{x}_J = A\hat{x}_J \tag{2.14a}$$

where $A = (a_{ij})$ contains the derivative values of all basis function in (2.1) at collocation points $\{t_k^{(j)}\}$ in (2.13), arranged in a level by level order. Specifically, if we order the basis function in (2.1) in an order set denoted as $\{\varphi_i^*(t)\}_{i=1}^N$ and the collocation points in an order set denoted as $\{t_i^*\}_{i=1}^N$, then

$$a_{ij} = \varphi^* i'(t_j^*), \quad 1 \leq i, j \leq N. \tag{2.14b}$$

For the system defined by (2.0a) and (2.0b), we expand the unknown function $x(t)$ for a given integer $J \geq 0$ and obtain

$$\begin{aligned} I_J x(t) &= I_{V_{b0}} x(t) + \sum_{j=0}^{J-1} I_{W_j} x(t) = x_{-1}(t) + \sum_{j=0}^{J-1} x_j(t) \\ &= x_J(t) \end{aligned} \tag{2.15}$$

where $x_{-1}(t)$ and $x_j(t)$, $0 \leq j \leq J-1$ have the same forms as those in (2.9) and (2.10), respectively. Interpolating $I_J x(t)$

in (2.15) at the collocation points $\{t_k^{(j)}\}$, $j \geq -1$ in (2.13) and substituting the expressions (2.15) into (2.0), we obtain the following nonlinear discrete algebraic system:

$$A\hat{x} = f(\hat{x}) \tag{2.16}$$

where A is an N-by-N invertible derivative matrix $\hat{x} = \hat{x}_J$, given in (2.11) and $f(\hat{x})$ is the vector of the values of $f(\hat{x})$ at all collocation points ordered in the same way as $\hat{x}$. For a given integer $J \geq 0$, A is a constant matrix. Solving (2.16) we obtain the solution $\hat{x}$ of the expansion coefficients. From a fast discrete wavelet transform (DWT) technique, we can effectively construct the approximation solution $x_J(t)$ of the ordinary differential equations (2.14) from the expansion coefficients $\hat{x}$ in a computation time $O(n \log n)$ [2]. The following two theorems summarize the presented FWCM's computational property.

Theorem 1: The FWCM has a convergence rate $O(h^4)$, where h is the distance between two adjacent collocation points (corresponding to the step length in the time-marching methods).

Theorem 2: The wavelets introduced are orthogonal wavelets which enable an adaptive scheme for the FWCM. The expansion coefficients can be calculated in a level-by-level adaptive fashion.

C. Derivative Matrix

Now we give the definition of derivative matrix A. Because of the multiresolution structure of spaces V_j, namely, $V_j \subset V_{j+1}$ and $V_J = V_0 \oplus W_0 \oplus \cdots \oplus W_J$, we can assume that $J = 0$ and that the wavelet interpolation $x_0(t) = I_0 x(t)$ for the function $x(t) \in H^2(I)$ can be written as the linear combination $x_0(t) = \sum_{k=-3}^{L-3} \hat{x}_k \varphi_k(t)$ of only the scaling functions in V_0.

Let $\{t_1, t_2, \ldots, t_N\}$ be the total collocation point, arranged here in an increasing order instead of level by level as in Section II-B, which is the union of partial set of collocation points $t^{(-1)}$ and $t^{(j)}$, $0 \leq j \leq J$ and $h_i = t_i - t_{i-1}$, $2 \leq i \leq N$, then the derivative matrix A is given as follows:

$$\begin{bmatrix} x'(1) \\ \cdot \\ \cdot \\ x'(N) \end{bmatrix} = H_1^{-1} H_2 \begin{bmatrix} x(1) \\ \cdot \\ \cdot \\ x(N) \end{bmatrix} = A \begin{bmatrix} x(1) \\ \cdot \\ \cdot \\ x(N) \end{bmatrix} \tag{2.17}$$

where

$$H_1 = \begin{bmatrix} \lambda_1 & 1 & & & & & & \\ \lambda_1 & 2 & \mu_1 & & & & 0 & \\ & \lambda_2 & 2 & \mu_2 & & & & \\ & & \cdot & \cdot & \cdot & & & \\ & & & \lambda_i & 2 & \mu_i & & \\ & & & & \cdot & \cdot & \cdot & \\ & 0 & & & & \lambda_{N-1} & 2 & \mu_{N-1} \\ & & & & & & 1 & \mu_{N-1} \end{bmatrix}_{(N+1)\times(N+1)} \tag{2.18}$$

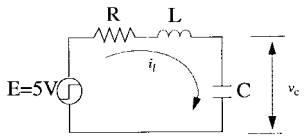

Fig. 5. A simple RLC circuit.

$$H_2 = \begin{bmatrix} a_1 & a_2 & a_3 & & & & & \\ c_1 & d_1 & e_1 & & & & 0 & \\ & \cdot & \cdot & \cdot & & & & \\ & & & & & & & \\ & & c_i & d_i & e_i & & & \\ & & & \cdot & \cdot & \cdot & & \\ 0 & & & & c_{N-1} & d_{N-1} & e_{N-1} & \\ & & & & b_3 & b_2 & b_1 & \end{bmatrix}_{(N+1)\times(N+1)} \tag{2.19}$$

and (2.19) at the bottom of this page where

$$\lambda_i = \frac{h_{i+1}}{h_i + h_{i+1}}, \quad \mu_i = 1 - \lambda_i \tag{2.20a}$$

$$a_1 = -\lambda_1 \frac{2+\mu_1}{h_1}, \quad a_2 = \lambda_1 \frac{2+\mu_1}{h_1} - \frac{(\mu_1)^2}{h_2}$$

$$a_3 = \frac{(\mu_1)^2}{h_2} \tag{2.20b}$$

$$b_1 = \mu_{N-1} \frac{2+\lambda_{N-1}}{h_N}, \quad b_2 = \frac{(\lambda_{N-1})^2}{h_{N-1}} - \mu_{n-1} \frac{2+\lambda_{N-1}}{h_N}$$

$$b_3 = -\frac{(\lambda_{n-1})^2}{h_{N-1}} \tag{2.20c}$$

$$c_i = -\frac{3\lambda_i}{h_i}, \quad e_i = \frac{3\mu_i}{h_{i+1}} \quad d_i = -c_i - e_i$$

$$2 \leq i \leq N-1. \tag{2.20d}$$

III. Numerical Experiments

This section shows several examples and compares the FWCM with the existing circuit simulation methods. We use a simple circuit, as shown in Fig. 5, and the ODE describing the circuit behavior is

$$\begin{bmatrix} \frac{dv_c}{dt} \\ \frac{di_l}{dt} \end{bmatrix} = \begin{bmatrix} 0 & 1/C \\ -1/L & -R/L \end{bmatrix} \begin{bmatrix} v_c \\ i_l \end{bmatrix} + \begin{bmatrix} 0 \\ 1/L \end{bmatrix} E \tag{3.0}$$

where v_c and i_l are, respectively, the capacitor's voltage and the inductance current.

Using the wavelet expansion of the variables v_c and i_l and the FWCM, we calculated the circuit response shown in Fig. 6. In the figure we plotted the approximated solutions by using up to zero ($j = 0$ base wavelet), one ($j = 1$), and two ($j = 2$) levels of wavelets. The FWCM needs ten collocation points for the scaling functions in V_o, 17 points for up to level-one wavelets, and 31 points for up to level-two wavelets. It is seen that the solution has been the same for the SPICE simulation for up to two levels of wavelet approximation.

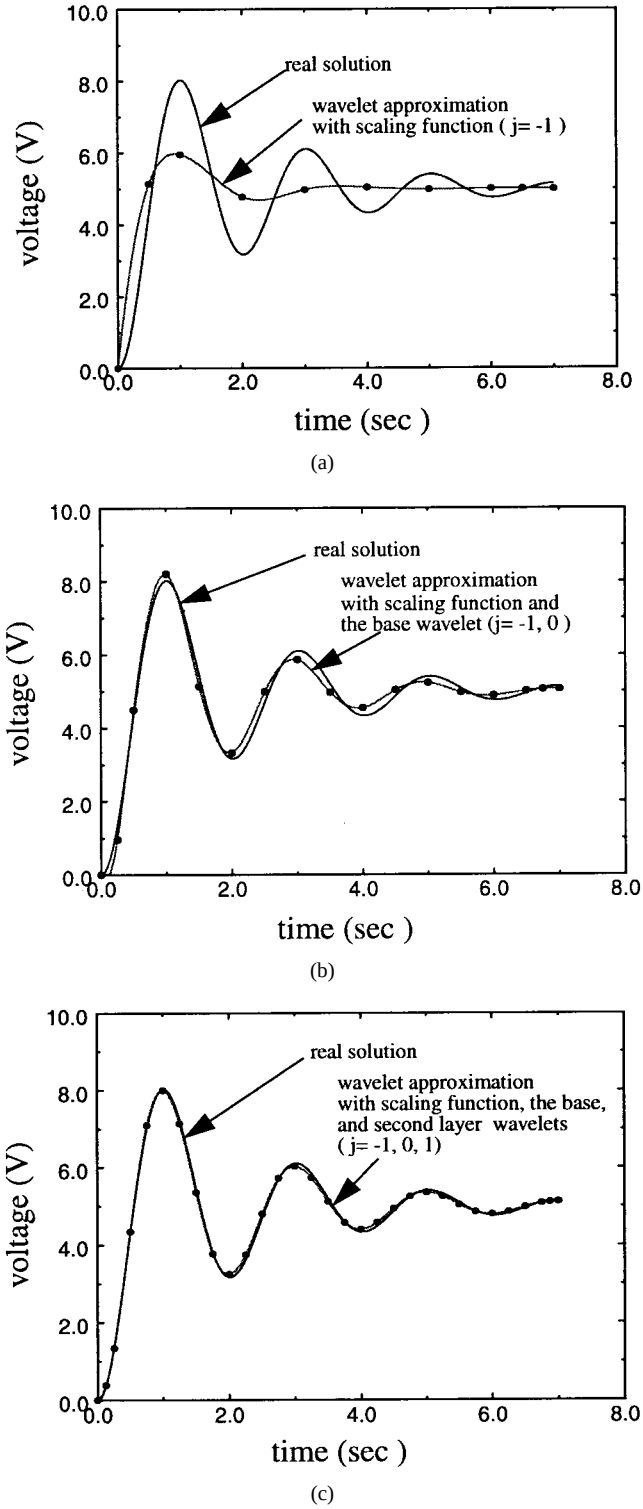

Fig. 6. The response of the circuit calculated by using the FWCM.

Fig. 7 shows the magnitude of expansion coefficient of different level wavelets. The coefficients of the third-level wavelets were very small. In practical computation, we can check the magnitude of the coefficient against a given parameter ε for the accuracy measurement and need not proceed to a higher level once the coefficients are smaller than ε. Notice also, that even at the same level, we do not have

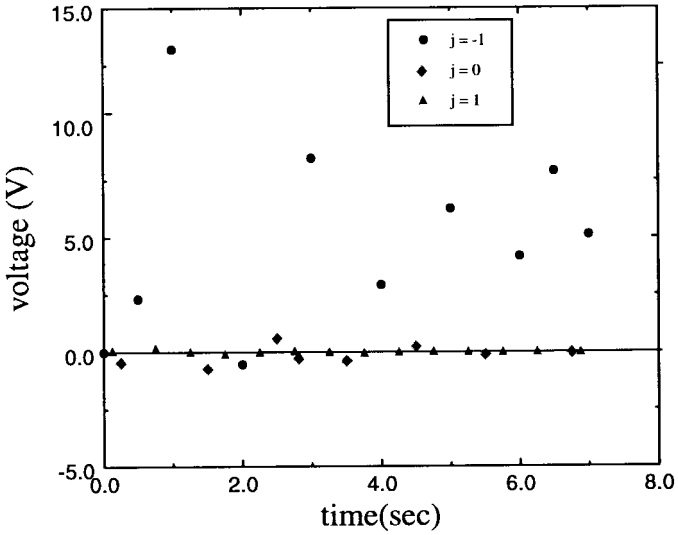

Fig. 7. The magnitudes of the collocation coefficients of the wavelets in different layers.

to insert wavelets over the entire interval. We need only add more wavelets at the location where accuracy has not been attained. Due to the wavelet localization property and Theorem 2, we can actually have an adaptive implementation of the FWCM by inserting wavelets level by level and location by location. Such an adaptive capability is crucial to the practical circuit simulation and the realization of the uniform approximation. Fig. 8 shows the solution by adding the second-level wavelets in the time range from 2.0 to 6.0 (not the entire time interval) to increase the accuracy of the solution obtained, by using only up to level-one wavelets. It is seen that accuracy in the time range concerned has been increased.

Fig. 9 compares the FWCM with the other simulation methods. In the figure we plotted the results from the SPICE simulation, the FWCM, the Euler backward method and the second-order Runge–Kutta method. The SPICE simulation is considered as the accurate solution, which is calculated by using more than 500 time steps. The FWCM uses 31 uniform collocation time points (up to two levels of wavelets). The Euler backward method uses 50 uniform time steps and the second-order Runge–Kutta method uses more than 31 variable time steps. Clearly, the FWCM produces a superior solution to those of the Euler and Runge–Kutta methods.

The result of the FWCM is more accurate than that of the Runge–Kutta method and can be explained by the difference of the convergence rate between the two algorithms. The FWCM has an $O(h^4)$ convergence rate, while the Runge–Kutta method used has only an $O(h^2)$ rate. In order to achieve the same accuracy, the Runge–Kutta method needs to use approximately 500 time steps (as in the SPICE simulation). In addition, the result from the Runge–Kutta method demonstrates a noticeable phase shifting if only 31 time steps are taken.

In our last example, we apply the FWCM to a stiff system presented in [4]. The system is described by the following

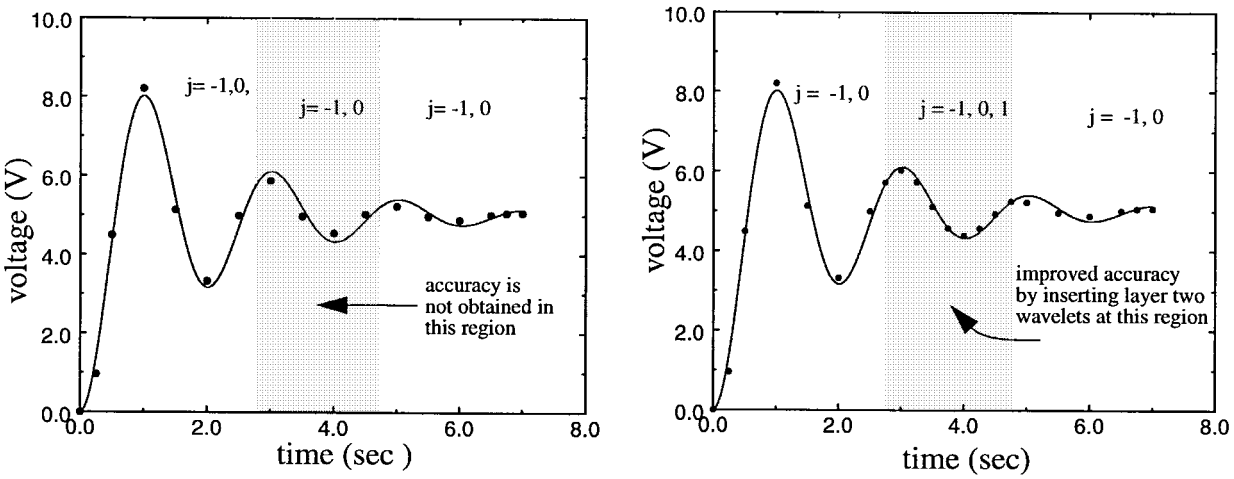

Fig. 8. Insertion of the layer two wavelets to increase the accuracy in a local region and the adaptive scheme.

ODE's:

$$\frac{du_1}{dt} = 9u_1 + 24u_2 + 5\cos t - \frac{1}{3}\sin t \tag{3.1a}$$

$$\frac{du_2}{dt} = -24u_1 - 51u_2 - 9\cos t + \frac{1}{3}\sin t \tag{3.1b}$$

and with the initial conditions

$$u_1(0) = \frac{4}{3} \tag{3.2a}$$

$$u_2(0) = \frac{2}{3}. \tag{3.2b}$$

The numerical calculation (Fig. 10) shows, again, that the FWCM produces a more accurate result than the compared time-marching methods for the same time steps.

IV. Discussion

We presented in this paper a new FWCM for high-speed circuit simulation. The paper explored the basic properties of the wavelet method for solving differential equations. Although in this paper only linear ODE's are discussed, the FWCM can be extended to the nonlinear case [11]. Furthermore, the FWCM can be applied to solve the nonlinear partial differential equations by expanding the space variables.

The paper is the first to use the wavelet method for circuit simulation. The experimental data are presented simply for demonstrating the feasibility and properties of the FWCM, not for showing its efficiency in practical circuit simulation. (All computational properties of the algorithm were proved theoretically in the [2].) Many implementation details and more benchmark testing are needed before the method becomes mature. The FWCM has demonstrated a promising direction in the development of high-speed VLSI simulation. We are investigating the use of this method to develop a practical VLSI simulator.

Appendix

Sobolev Spaces: During discussion of the FWCM, the following properties of Sobolev spaces are required. Further details can be found in Adams [5].

Let I denote a standard interval, say $I = [0, L]$, $L > 4$, and $H^2(I)$ denote the following Sobolev space:

$$H^2(I) = \{x(t),\ t \in I \mid \|x^i\|_2 < \infty,\ i = 0, 1, 2\} \tag{A.1}$$

where $x^i = \frac{d^i x}{dt^i}$ and

$$\|x^i\|_2 = \sqrt{\langle x^i, x^i \rangle}, \qquad i = 0, 1, 2 \tag{A.2}$$

while

$$\langle x^i, y^i \rangle = \int_I x^i(t) y^i(t)\, dt, \qquad i = 0, 1, 2. \tag{A.3}$$

It can be easily checked that $H^2(I)$ is a Hilbert space, equipped with the inner product

$$\langle x, y \rangle = \sum_{i=0}^{2} \int_I x^i(t) y^i(t)\, dt. \tag{A.4}$$

We have the inner-product norm of $H^2(I)$

$$\|x\|_2 = \sqrt{\langle x, x \rangle} = \left(\sum_{i=0}^{2} \int_I |x^i(t)|^2\, dt \right)^{1/2}. \tag{A.5}$$

We say a function $x \in H_0^2(I)$ if $x \in H^2(I)$ and $x(0) = x(L) = x'(0) = x'(L) = 0$. It can also easily be checked that $H_0^2(I)$ is a Hilbert space equipped with the following inner product:

$$\langle x, y \rangle = \int_I x''(t) y''(t)\, dt. \tag{A.6}$$

The corresponding norm induced by the inner product (A.6) is

$$|x|_2 = \sqrt{\langle x'', x'' \rangle}. \tag{A.7}$$

We now mention some properties of the space $H^2(I)$, which have been used in the paper.

(i) $H^2(I)$ is a separable Hilbert space equipped with the inner product (A.4).

(ii) A complete orthonormal system in a separable Hilbert space H is a sequence $\{e_i\}_{i=1}^{\infty}$ of the element satisfying

$$\langle e_i, e_j \rangle = \delta_{ij}, \delta_{ij} = \begin{cases} 1, & \text{if } i = j \\ 0, & \text{if } i \neq j \end{cases} \tag{A.8}$$

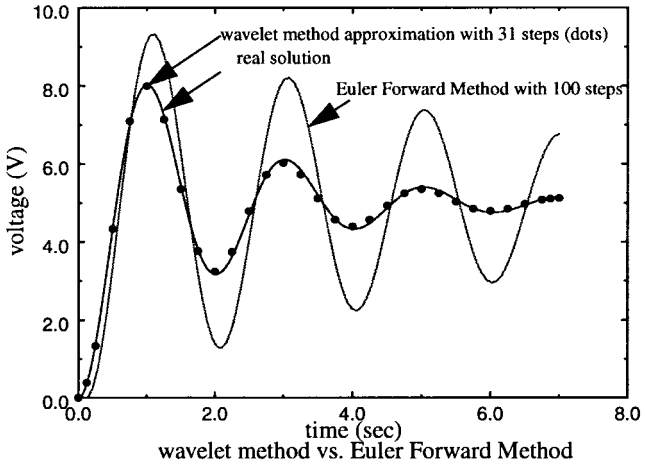

(a)

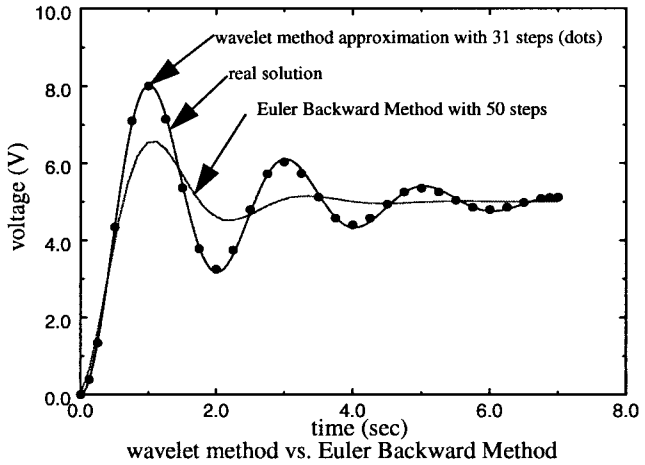

(b)

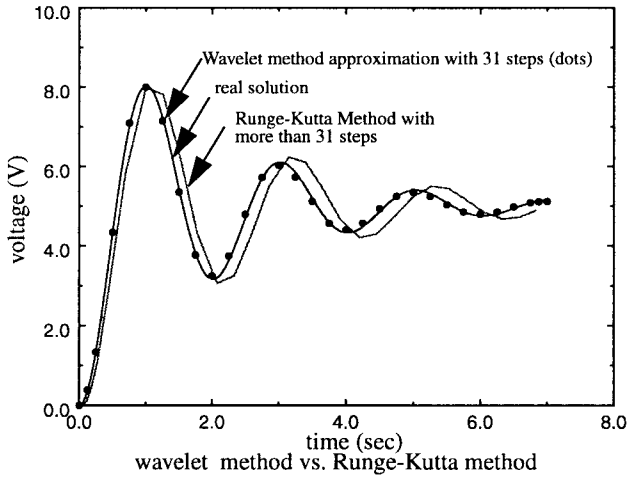

(c)

Fig. 9. Comparison of the FWCM with the other simulation methods.

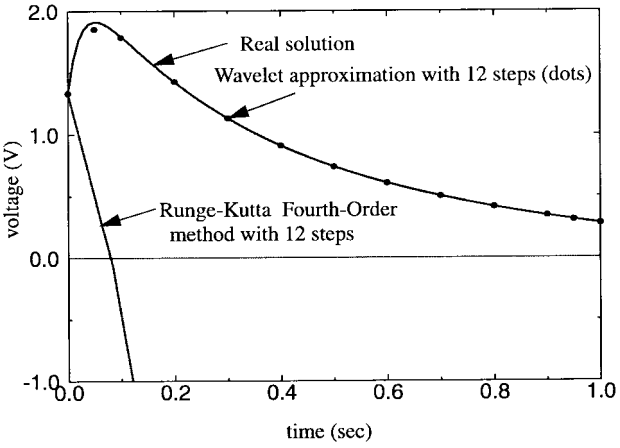

(a)

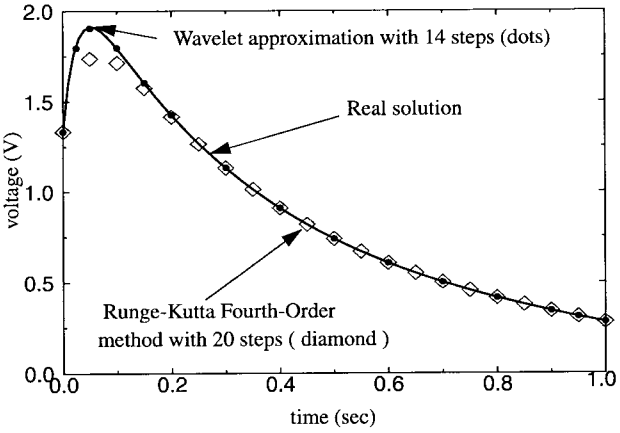

(b)

Fig. 10. The property of the uniform approximation.

and such that for each $x \in H^2(I)$ we have the following Parseval identity:

$$||x||^2 = \sum_{i=1}^{\infty} \langle x, e_i \rangle^2. \tag{A.9}$$

(iii) Let M be a closed subspace of the Hilbert space $H^2(I)$. Then, for every $x \in H^2(I)$ we have $x = u + v$ where $u \in M$ and $v \in M^{\perp}$ are uniquely determined by x and

$$M^{\perp} = \{v \in H^2(I) \mid \langle u, v \rangle = 0, \qquad \text{for all } u \in M\}$$

is the orthogonal complement of M, denoting $M \perp M^{\perp}$. We have $H^2(I) = M \oplus M^{\perp}$ where the symbol $\oplus$ stands for a direct sum.

Finally, we define the support of a function x as

$$\text{supp}x = \{t \in (0, L), x(t) \neq 0\}.$$

We say that x has a compact support in I if the closure of $\text{supp}x$ is in I. As we know, any wavelet basis function in the FWCM has a compact support.

REFERENCES

[1] D. Zhou, N. Chen, and W. Cai, "A fast wavelet collocation method for high-speed VLSI circuit simulation," in *Proc. ICCAD 95*, 1995, San Jose, CA, pp. 115–122.
[2] W. Cai and J. Z. Wang, "Adaptive multi-resolution collocation methods for initial boundary value problems of nonlinear PDE's," *SIAM J. Numer. Anal.*, Vol. 33, no. 3, pp. 937–970, 1996.
[3] L. O. Chua and P. M. Lin, *Computer-Aided Analysis of Electronic Circuits: Algorithms, and Computational Techniques*. Englewood Cliffs, NJ: Prentice-Hall, 1975.
[4] R. L. Burden and J. D. Faires, *Numerical Analysis*. PWS, 1993.
[5] R. A. Adams, *Sobolev Spaces*. New York: Academic, 1975.
[6] I. J. Schoenberg, *Cardinal Spline Interpolation* (CBMS-NSF Series in Applied Mathematics 12). Philadelphia, PA: SIAM, 1973.

[7] D. Zhou, X. Q. Li, W. Zhang, and W. Cai, An Adaptive Wavelet Method for Nonlinear Circuit Simulation, in *Proc. ICCAD-96*, to be published.
[8] L. T. Pillage and R. A. Rohrer, "Asymptotic waveform evaluation for timing analysis, *IEEE Trans. Computer-Aided Design*, vol. 9, pp. 352–366, Apr. 1990.
[9] S. Lin and E. S. Kuh, "Pade approximation applied to transient simulation of lossy coupled transmission lines," in *Proc. IEEE Multi-Chip Module Conf.*, Santa Cruz, CA, Mar. 1992.
[10] K. Singhal and J. Vlach, "Computation of Time Domain Response by Numerical Inversion of the Laplace Transform," *J. Franklin Inst.*, vol. 299, no. 2, pp. 109–126, Feb. 1975.
[11] D. Zhou, W. Cai, and W. Zhang, "An adaptive wavelet method for nonlinear circuit simulation," submitted to *IEEE Trans. Computer-Aided Design*, vol. 46, Aug. 1996.
[12] I. Daubechies, *Ten Lectures on Wavelet*. Philadelphia, PA: SIAM, 1992.
[13] S. Bertoluzza and G. Naldi, "A wavelet collocation method for the numerical solution of partial differential equations," *Appl. and Comput. Harmon. Anal.*, vol. 3, pp. 1–9, 1996.

Dian Zhou received the B.S. degree in physics and the M.S. degree in electrical engineering from Fudan University, Fudan, R.O.C., in 1982 and 1985, respectively, and the Ph.D. degree in electrical and computer engineering from the University of Illinois at Urbana-Champaign, in 1990.

He joined University of North Carolina at Charlotte in 1990, where he has been an Associate professor since 1995. His research interests include: high-speed VLSI systems, and CAD tools and algorithms.

Dr. Zhou received the Research Initiation Award from National Science Foundation in 1991, the IEEE Circuits and Systems Society Darlington Award in 1993, and the National Science Foundation Young Investigator Award in 1994. He also served as a panel member of the NSF CAREER Award in 1996. He was a Guest Editor for the *International Journal of Custom-Chip Design, Simulation and Testing*, and was an Associate Editor for IEEE TRANSACTIONS ON CIRCUITS AND SYSTEMS.

Wei Cai received the Ph.D. degree in applied mathematics from Brown University, Providence, RI in 1989.

He joined the Department of Mathematics, the University of North Carolina at Charlotte in 1995 where he was an Assistant Professor and later an Associate Professor. In 1995 he joined the Department of Mathematics, the University of California at Santa Barbara as an Assistant Professor and later an Associate Professor II. In 1996, he joined the Department of Mathematics at the University of North Carolina at Charlotte. His research interests includes numerical methods and scientific computations for reacting flow simulation and computational electromagnetics. Currently, he is involved in the development of numerical methods for the deflagration to detonation transition (DDT) and algorithms development for electromagnetic calculations and parameter extraction for computer packaging and VLSI simulations.

Dr. Cai is a member of SIAM.